4A.2 OBSERVATIONS OF WALL CLOUD FORMATION IN SUPERCELL THUNDERSTORMS DURING VORTEX2

Nolan T. Atkins, Eva M. Glidden, and Timothy M. Nicholson
Lyndon State College, Lyndonville, Vermont 05851

1. INTRODUCTION

The wall cloud is a lowering of cloud base associated with the updraft of a thunderstorm. The focus of this study concerns wall clouds formed within supercell thunderstorms (Bluestein 1983; Davies-Jones 1986; Bluestein 1993). Early observational studies suggested that the supercell wall cloud is the visual indicator of a strong updraft core and may exhibit cyclonic rotation. (Moller et al. 1978; Bluestein 1984). Recent studies have also revealed the existence of anticyclonic wall clouds (Atkins et al. 2012). National Weather Service storm spotter training documents indicate that persistent wall clouds that develop strong rotation and exhibit rapid upward vertical motion are often regarded as precursors to tornadogenesis (http://www.nws.noaa.gov/om/brochures/adv_spotters.pdf). While many studies of supercell thunderstorms have photo-documented the wall cloud, amazingly little is known about their formation.

Our current understanding of wall cloud formation is based on idealized modeling results of Rotunno and Klemp (1985) and visual observations. In their idealized simulation of a supercell, Rotunno and Klemp (1985) showed that the air entering the storms updraft region where the wall cloud formed was being ingested from behind the gust front. This rain-cooled air had descended from mid levels within the storm and subsequently saturated below the primary cloud base as it ascended with the low-level updraft that was dynamically forced by an upward directed pressure gradient. Observations by storm intercept teams have since confirmed that cloud tags associated with cooler air behind the gust front often rise into the updraft. Often this occurs near or in association with the distinct “tail cloud” that protrudes from near the base of the wall cloud toward the cooler air. This mechanism is described in National Weather Service storm spotter training documents (http://www.nws.noaa.gov/training/wxspot.php).

To date, no observational study has been published confirming the Rotunno and Klemp (1985)

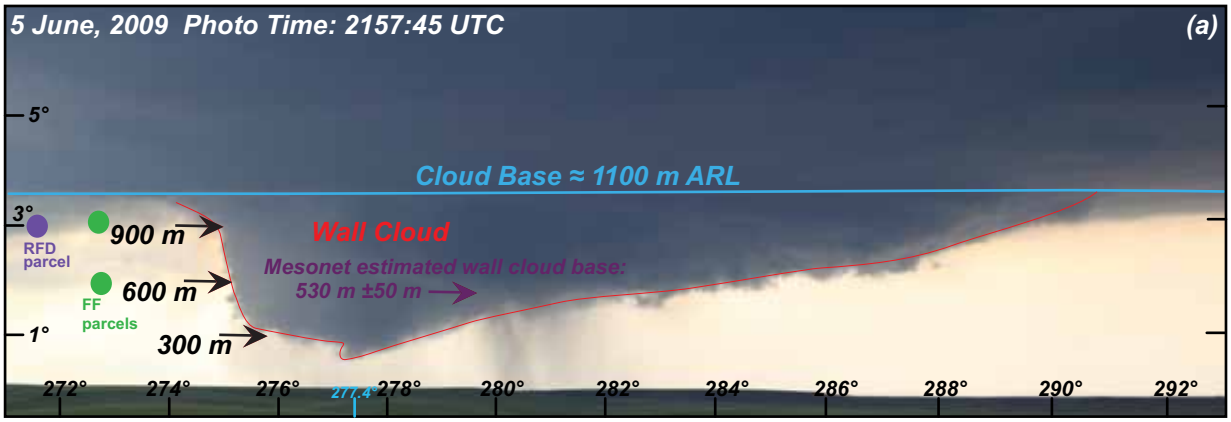

FIG 1. Photograph of the wall cloud taken at 2157:45 UTC on 5 June 2009. Photogrammetric estimates of cloud base height and wall cloud vertical extent are shown in black. Mobile mesonet estimated wall cloud base height is shown in purple. Wall cloud boundary is shown in red.

Corresponding author address: Nolan T. Atkins, Department of Atmospheric Sciences, Lyndon State College, Lyndonville, VT 05851
E-mail: nolan.atkins@lyndonstate.edu

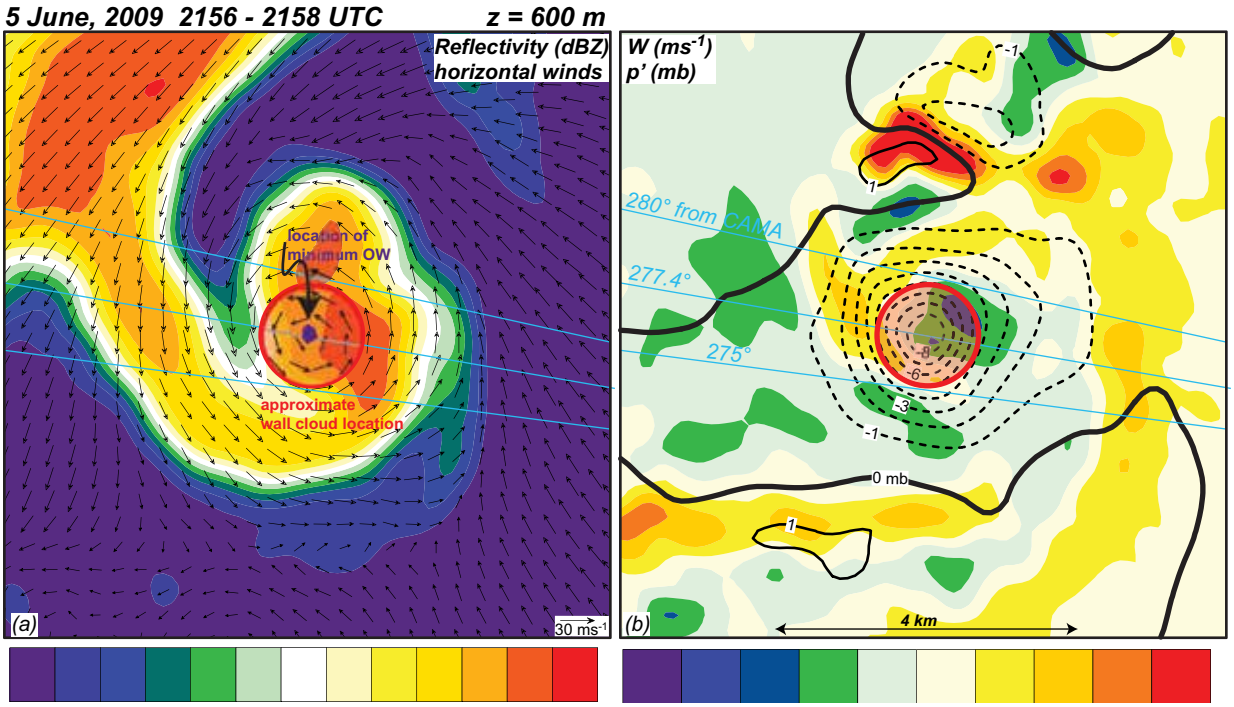

FIG 2. Dual-Doppler data from 2156:00 – 2158:00 UTC at 600 m ARL is shown. (a) Radar reflectivity from DOW 7 (color) and dual-Doppler winds (ms^{-1}; black vectors). Cyan lines are the left, center, and right azimuths of the estimated wall cloud location based on photogrammetry. The thick red line is the approximate wall cloud location. The location of minimum Okubo-Weiss number is filled purple. (b) Vertical velocity (ms^{-1}; color) and perturbation pressure (black contours) are shown. Wall cloud location and azimuths are same as in (a).

mechanism for wall cloud formation. It is not known what fraction of air creating observed wall clouds originates in the storm mid levels or from other source regions such as the inflow. Given that some wall clouds may be collocated with the low-level mesocyclone and therefore contain significant low-level rotation, it is possible that some or all of the wall cloud lowering is created by the adiabatic cooling associated with the pressure deficit at the circulation center. While this mechanism may not explain all of the lowering for wall clouds associated with weak rotation, it may explain a significant portion of the lowering associated with strongly rotating wall clouds. No study has systematically examined this wall cloud formation mechanism.

2. VORTEX2

The requisite visual, kinematic, and thermodynamic data to examine the aforementioned wall cloud formation mechanisms was collected during the Verification of the Origins of Rotation in Tornadoes Experiment II (VORTEX2). VORTEX2 was a large multi-agency field project designed to collect observations in and around supercell thunderstorms. To increase the number of storm intercepts, the experiment was mobile covering the Southern, Central, and Northern Plains states during the spring seasons of 2009 and 2010. More information on VORTEX2 can be found in the review article by Wurman et al. (2012).

Analyses of two supercells observed during VORTEX2 are presented herein. The first formed on 5 June 2009 over Goshen CO Wyoming (hereafter referred to as the Goshen County supercell). This supercell produced a well-defined wall cloud and attendant EF-2 tornado. The second supercell was observed on 11-12 June 2009 west-northwest of La Junta CO (hereafter referred to as the La Junta supercell). While this supercell was tornado warned during the time of VORTEX2 data collection, it did not spawn a tornado despite producing a well-defined wall cloud.

3. DATA ANALYSIS METHODS

The wind field in and around the wall clouds was generated from dual-Doppler synthesis of radial

velocities collected by the mobile X-band Doppler On Wheels (DOW) 6 and 7 radars operated by the Center for Severe Weather Research (CSWR; Wurman 2001). After the data were edited and navigated, it was objectively interpolated to a Cartesian grid using a two-pass Barnes scheme. The horizontal and vertical grid spacing was set to 100 m over a 15 km x 15 km horizontal domain. Vertical velocities were calculated by upward integration of the mass continuity equation. Dual-Doppler volumes were collected every two minutes. Examples of dual-Doppler wind syntheses from VORTEX2 data and further details of the dual-Doppler technique can be found in Markowski et al. (2012a, b), Atkins et al. (2012), and Kosiba et al. (2013).

The thermodynamic properties of low-level parcels entering the wall cloud, was based on mobile mesonet (Waugh and Fredrickson 2010) observations. The mobile mesonets carried roof-mounted instrumentation that included temperature, relative humidity, and pressure sensors along with a three-cup anemometer. All data, including GPS derived latitude and longitude, were collected at one-second intervals. Data collected within the window of five minutes before and after the dual-Doppler analysis time were used in the analyses. It was assumed that storm evolution was not significant during this ten-minute time period. All mobile mesonet data were space-time adjusted to account for storm motion.

The visual extent and evolution of the wall clouds was determined by photogrammetry analysis of still images captured by two photo teams. Photogrammetry is the process of superimposing azimuth and elevation angle grids on photographs by computing or determining the precise azimuths of landmarks in the horizon relative to the photographer. Once the landmark locations are known, the effective focal length and tilt angle of the photograph can be computed. Spherical trigonometry is then used to create the azimuth-elevation grid. Once the photo has been gridded, it can then be combined

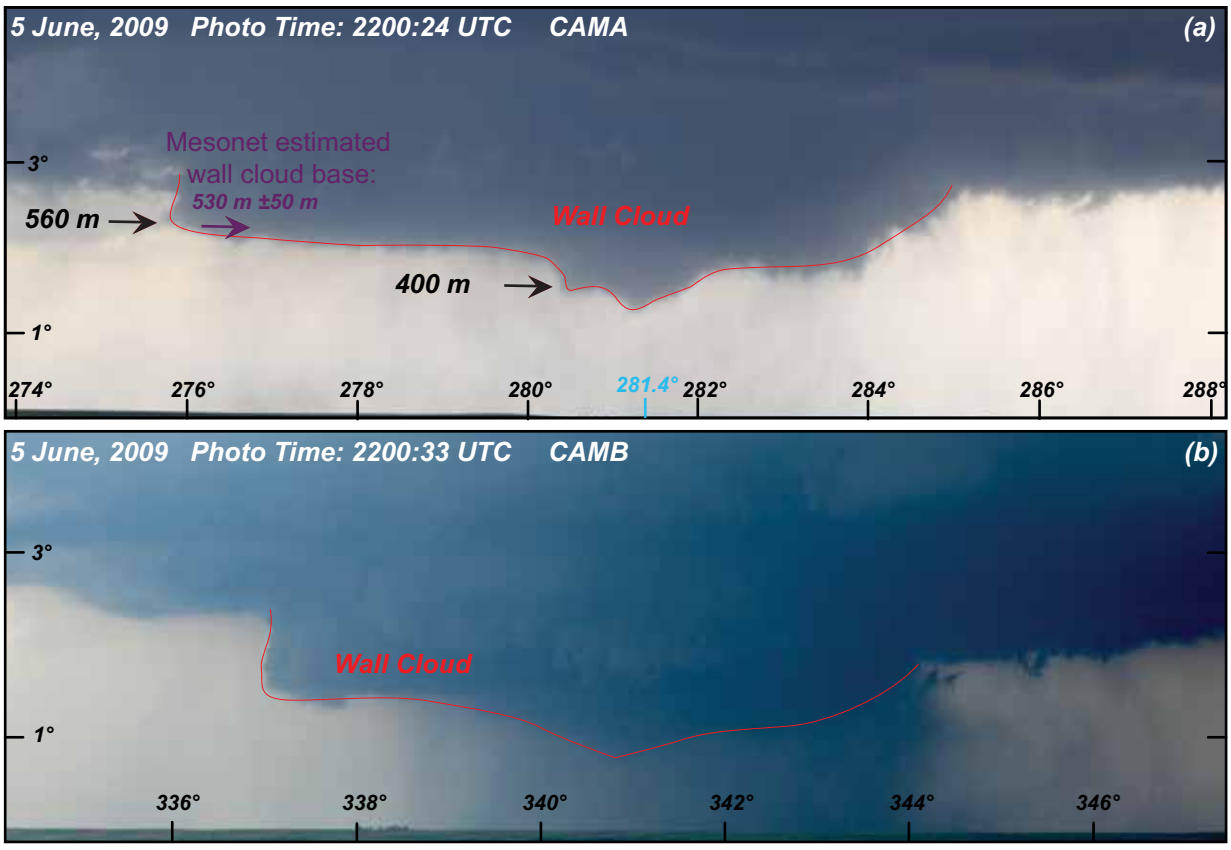

FIG 3. Photographs of the wall cloud taken at (a) 2200:24 UTC from the CAMA and (b) 2200:33 UTC from the CAMB locations, respectively on 5 June 2009. Photogrammetric and mobile mesonet estimates of wall cloud base height are shown in black and purple, respectively. Wall cloud boundary is shown in red.

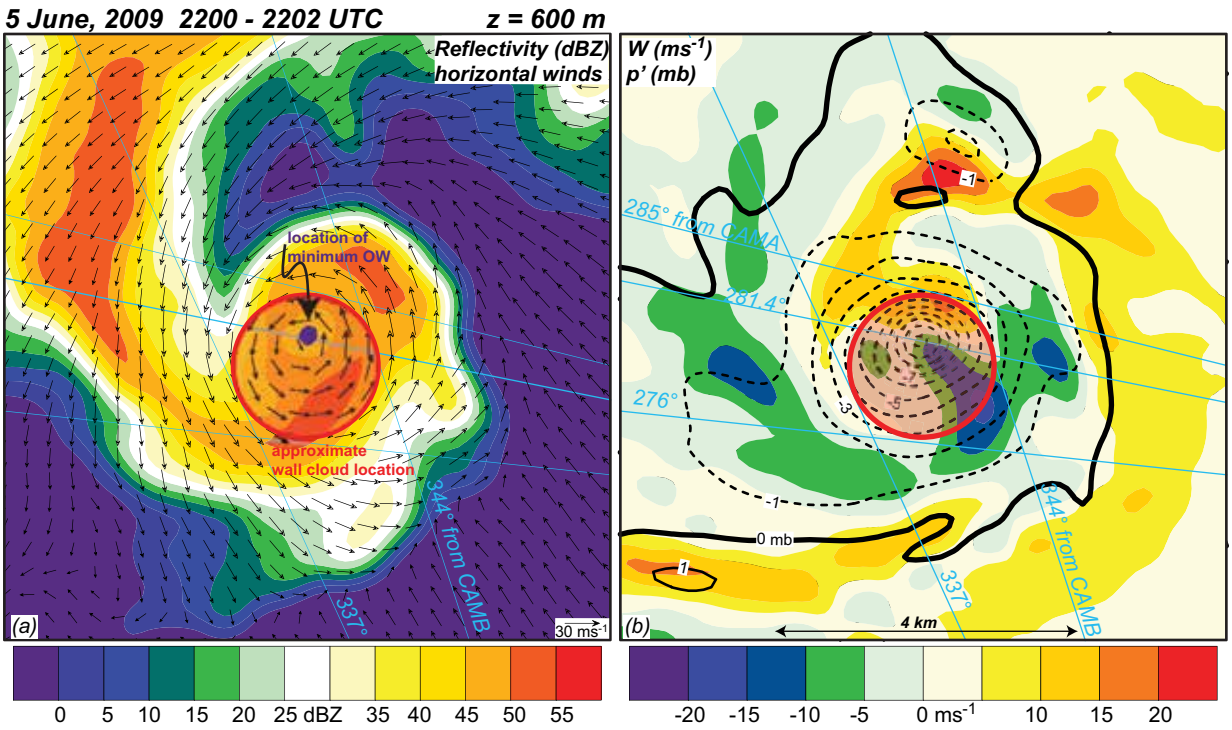

FIG 4. Same as Fig. 2 except for the time period 2200:00 – 2202:00 UTC.

with the dual-Doppler wind field and radar reflectivity observations. More details on photogrammetry can be found in Wakimoto et al. (2011) and Atkins et al. (2012).

4. GOSHEN COUNTY TORNADIC WALL CLOUD

4.1 Visual and Dual-Doppler Observations

The Goshen County wall cloud observed at 2157:45 UTC is shown in Fig. 1. The view in Fig. 1 is from the DOW7 location on highway 85 looking to the west (see Fig. 1 in Wakimoto et al. (2011) for the radar and photo team locations relative to the hook echo). The wall cloud was approximately 17 km from the radar/photo location. A radar-detected tornado formed at about 2152 UTC but was not yet visible. The wall cloud lowering was centered on azimuths 276-278° and extended nearly 800 m below the primary cloud base of 1100 m above radar level (ARL; relative to DOW 7). The primary cloud base was determined photgrammetrically and with a nearby inflow sounding (not shown). The wall cloud lowering was asymmetric as it gradually rose to the north. Rain curtains were observed to the north and south of the wall cloud suggesting that it was embedded within precipitation. The location of the wall cloud relative to the hook echo is shown in Fig. 2. Consistent with Fig. 1, the wall cloud was embedded in precipitation that was wrapping around and embedded in the low-level mesocyclone (Fig. 1a). Video (not shown) revealed that the wall cloud contained significant rotation. The strongest rotation in the dual-Doppler data was located by computing and locating the minimum Okubo-Weiss number (Okubo 1970; Weiss 1991; Markowski et al. 2011). It was located at an azimuth of 277.4 degrees from the DOW7/photo location (Fig. 2) near the wall cloud center. The wall cloud lowering was located at the same azimuth (Fig. 1).

It has long been accepted and shown by Rotunno and Klemp (1985) that the wall cloud is embedded within low-level updraft. The updraft is necessary to dynamically force the negatively buoyant evaporatively-cooled air to wall cloud base. The wall cloud position relative to the vertical velocity field in Fig 2b suggests that the wall cloud is on the gradient of vertical velocity and contains some downdraft air on the southern and eastern flanks. This downdraft air is likely associated with the rear-flank downdraft (RFD) that is wrapping around the southern side of the wall cloud. It has been hypothesized that the RFD may play a role in tornadogenesis (e.g., Lemon and Doswell 1979). The relationship between the RFD, tornado, low-level mesocyclone, and wall cloud, is poorly understood.

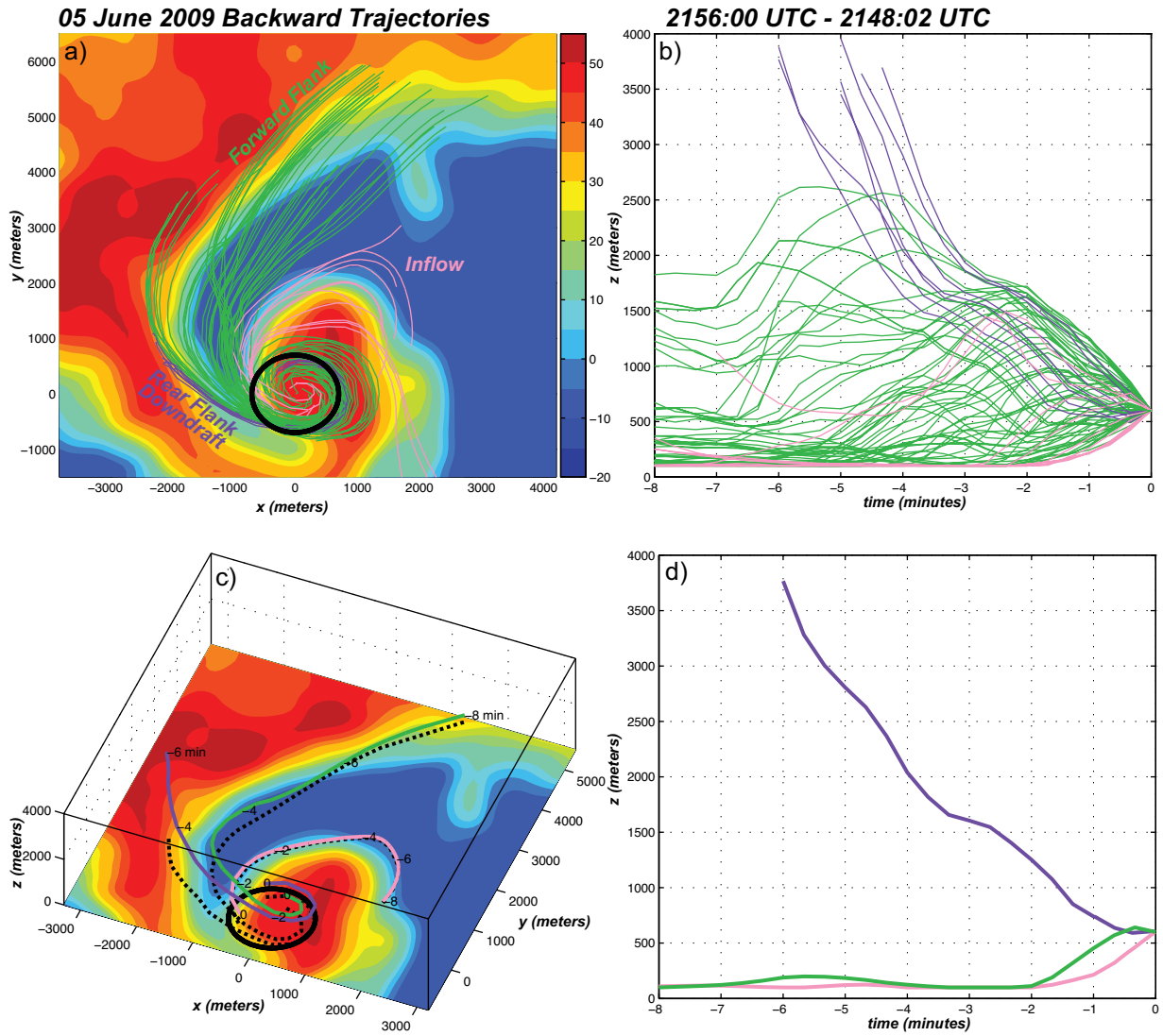

FIG 5. Radar reflectivity from DOW 7 (color; 500 m ARL) and backward trajectories for parcels entering the wall cloud. The radar reflectivity data is from the 2156:00 – 2158:00 dual-Doppler analysis. Backward trajectories were calculated from 2156:00 to 2148:02 UTC. (a) Plan view of radar reflectivity and trajectories. Inflow, forward flank, and rear-flank downdraft parcels are colored pink, green, and purple, respectively. The approximate wall cloud location is shown in black. (b) Height versus time plot of the trajectories shown in (a). (c) Three-dimensional perspective of the radar reflectivity field shown in (a) along with representative parcel trajectories from the inflow, forward flank, and rear-flank downdraft locations. Black dashed lines represent the ground-relative location of the respective trajectories. Black time labels are minutes before the initial time of 2156:00 UTC. (d) Height versus time diagram of the three representative trajectories shown in (c).

Similar results were observed a couple minutes later with photos taken at 2200:24 and 2200:33 UTC at the DOW7 and DOW6 locations, respectively. Much of the wall cloud base was found at about 560 m ARL (Fig. 3a). An additional 160 m of lowering was observed just north of the wall cloud center. It was possible to triangulate the wall cloud location in Fig. 3 and superimpose the position on the radar data collected from 2200 - 2202 UTC. As shown in Fig. 4 and consistent with the results in Fig. 2, the wall cloud was located in a region of precipitation associated with the hook echo and appeared to be located within the low-level mesocyclone. Notice that the strongest rotation was not located at the

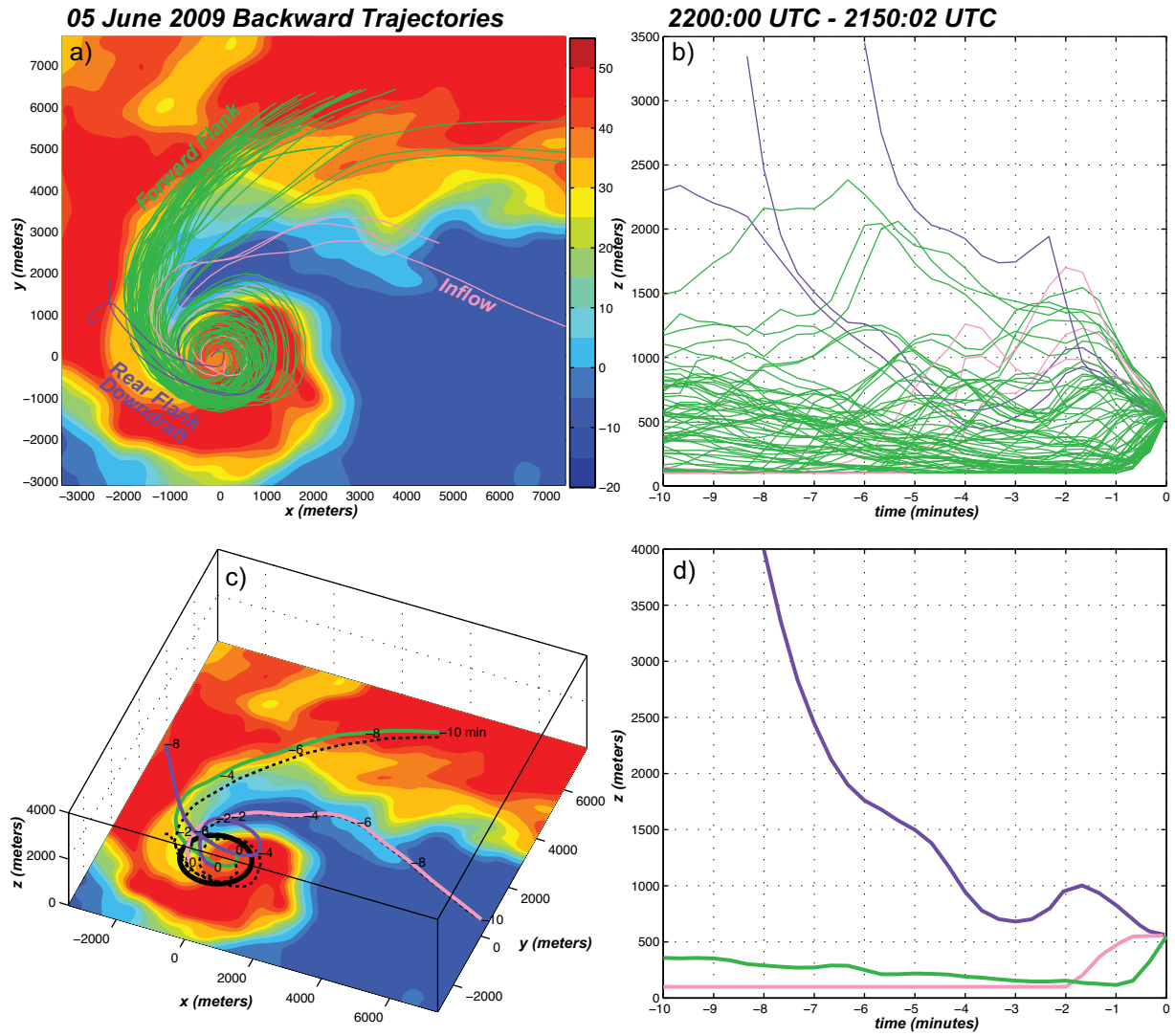

FIG 6. Same as Fig. 5 except that the trajectories were run from 2200:00 – 2150:02 UTC and the radar reflectivity was generated from a dual-Doppler analysis valid from 2200:00 – 2202:00 UTC.

center of the wall cloud. Rather, it was displaced to the north and was collocated with the local wall cloud lowering shown in Fig. 4. This was the location of the developing tornado. The tornado funnel cloud made visual contact with the ground at about 2206 UTC.

As with the wall cloud in Fig.1, the wall cloud at 2200 UTC was partially embedded in downdraft. (Fig. 4b). It appeared to be the rear-flank downdraft that wrapped around the southern and eastern side of the wall cloud.

4.2 Wall Cloud Parcel Source Regions

In order to test the wall cloud formation hypothesis put forth by Rotunno and Klemp (1985), it is necessary to identify regions of the storm from which parcels entering wall cloud base are coming from. This was partially accomplished by calculating backward parcel trajectories for hundreds of parcels entering the wall cloud base. Trajectories were computed by interpolating the dual-Doppler data every 20 seconds in time. Spatial interpolation was trilinear. Results of this analysis are shown in Fig. 5 for the wall cloud observed at 2157:45 in Fig. 1. The parcel trajectories were computed backward in time for ten minutes and were released within the wall cloud location shown in Fig. 2 at a height of 550 m ARL. The trajectories in Fig. 5a,c illustrate that parcels entering the wall cloud come from three source regions. They are the inflow, rear-flank downdraft, and the forward flank with the majority coming from

the forward flank region. The inflow parcels originated at low levels, wrapping around the northern and western flanks before ascending to wall cloud base (Fig. 5b,d).

It was surprising to observe a number of parcels reaching cloud base that had descended in downdraft. A few parcels descended within the rear-flank downdraft while others originated in the forward-flank region at altitudes greater than 1000 m ARL and then descended to wall cloud base (Fig. 5b). The fact that parcels were descending to wall cloud base is consistent with the results shown in Figs. 2b. and 4b. Namely, the wall cloud was partially embedded in downdraft. It is not known how these parcels are descending. One might expect that they are descending moist adiabatically. The microphysical characteristics of the supercell rear-flank downdraft, however, are poorly understood. The remaining forward flank parcels originated at low-levels (Fig. 5b,d) and ascended to wall cloud base in a manner consistent with the idealized modeling results of Rotunno and Klemp (1985).

Parcel trajectories entering the wall cloud at 2200 UTC (Fig. 4) were computed to examine the generality of the results shown in Fig. 5. These trajectories are shown in Fig. 6 and are consistent with the results in Fig. 5. Additional analyses of a supercell wall cloud that exhibited weak rotation on 26 May 2010 also revealed the same three wall cloud source regions (not shown).

4.3 Wall Cloud Formation

The question of wall cloud formation is now addressed. The requisite data exists to test the hypothesis put forth by Rotunno and Klemp (1985) that evaporatively cooled air in the forward flank region saturates at a lower altitude as it is ingested in the updraft. Indeed, Figs. 5 and 6 showed that low-level air in the forward flank region entered wall cloud base. The thermodynamic properties of this air can be approximated with the mobile mesonet data (Fig. 7) despite the sparse coverage in and around the hook echo due to the limited road network over southeastern Wyoming. The rear and forward flank regions appear to be about 3-4 K virtually cooler and about 1 g kg^{-1} drier than the inflow as partially sampled by the mobile mesonet (Fig. 7) and a nearby mobile sounding (not shown). The potential temperature and mixing ratio deficits in the forward flank region where the parcels entering wall cloud base originate (gray shaded region in Fig. 7) were approximately 4.0 K and 1.5 g kg^{-1} relative to the inflow, respectively. Assuming adiabatic ascent,

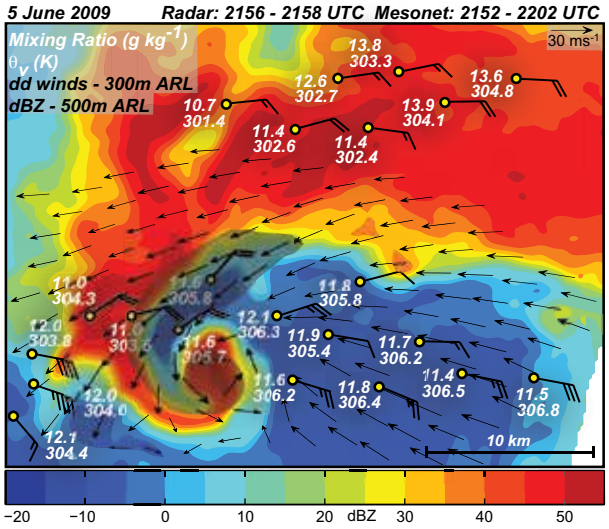

FIG 7. Radar reflectivity from DOW 7 (color; 500 m ARL) and dual-Doppler winds (black vectors; 300 m ARL) from 2156:00 – 2158:00 UTC. Mobile mesonet winds (black barbs; ½ flag = 5 ms^{-1}, full flag = 10 ms^{-1}), mixing ratio (g kg^{-1}), and virtual potential temperature (K) are shown from 2152:00 – 2202:00 UTC. The semi transparent region represents the location of forward-flank parcel trajectories shown in Fig. 5.

these low-level forward flank parcels would saturate at approximately 530 m ARL. This altitude is nearly identical to the observed wall cloud base of 560 m ARL at 2200:24 and 2200:33 UTC (Fig. 3) and is within the range of 300-900 m ARL for the sloping wall cloud at 2157:45 UTC.

Apparent in Fig. 3a is the localized lowering just north of the wall cloud center. This lowering is evident in Fig. 3a between azimuths of 280 and 282 degrees. It extended about 150-160 meters below the primary wall cloud base. It is hypothesized that this lowering was associated with the pressure deficit associated with the rotation in the wall cloud. A pressure retrieval using the dual-Doppler wind field was performed using techniques established by Gal-Chen (1978) and Hane and Ray (1985). The perturbation pressure fields are shown in Figs. 2b and 4b for the 2156-2158 UTC and 2200-2202 UTC volume scans, respectively. In Fig. 2b, the lowest pressure perturbation was approximately -8 mb and was centered on an azimuth of 277.4 degrees. The lowest extent of the wall cloud was observed at 2257:45 UTC at this same azimuth (Fig. 1). The pressure perturbation in Fig. 4b was about -10 mb, centered on 281.4 degrees. The localized lowering

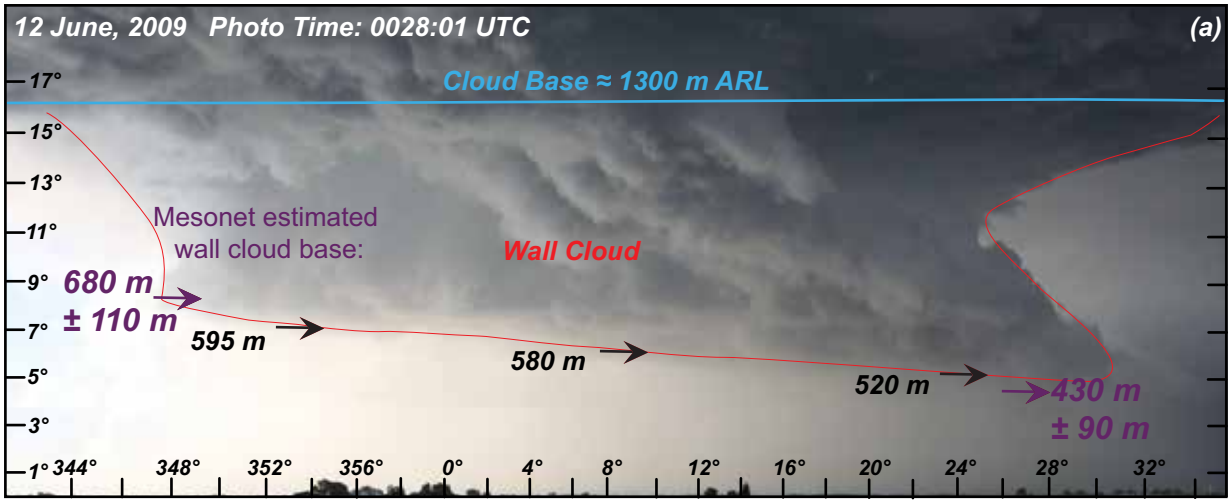

FIG 8. Photograph of the wall cloud taken at 0028:01 UTC on 12 June 2009. Photogrammetric estimates of cloud base height and wall cloud vertical extent are shown. Mobile mesonet estimated cloud base height is shown in purple. Photogrammetric estimated cloud base in shown in black. Wall cloud boundary is shown in red.

in Fig. 4b was located between azimuths of 280-282 degrees. Thus, the lowest portion of the wall cloud base is collocated with the lowest pressure within the wall cloud. Assuming that the air near wall cloud base is close to or saturated, a -10 mb pressure drop would result in about 140 m of lowering using the US Standard Atmosphere. Thus, the pressure deficit within the wall cloud can explain nearly all of local lowering observed in Fig. 3. It is possible that the pressure deficit is larger than what is shown in Figs. 2 and 4 since circulation on the tornado scale is not resolved in the dual-Doppler wind field.

5. LA JUNTA NON TORNADIC WALL CLOUD

5.1 Visual and Dual-Doppler Observations

A well-defined wall cloud at 0028:01 UTC was observed with a supercell sampled by the VORTEX2 teams on 12 June 2009 west-northwest of La Junta, CO (Fig. 8). The wall cloud extended 700-750 m below the primary cloud base. Wall cloud base varied from approximately 520 to 600 m ARL from northeast to southwest (Fig. 8). There are notable differences between the wall clouds observed on 5 and 11-12 June 2009. First, triangulation of photographs placed the La Junta wall cloud to the south of the storms precipitation region. This is in contrast to the 5 June 2009 wall cloud that was embedded in precipitation wrapping around the low-level mesocyclone. Also notice that the La Junta wall cloud was not collocated with the low-level mesocyclone. The dual-Doppler analysis and WSR-88D observations from near Pueblo CO suggested that the mesocyclone was approximately 3 km to the northwest of the wall cloud (Fig. 9a). The mesocyclone was relatively weak, consistent with the lack of a well-defined hook echo at the time shown in Figs. 8 and 9. Video observations confirmed that the wall cloud was not rotating at 0028 UTC. These observations suggest that the La Junta supercell had produced strong outflow that had displaced the updraft from the mesocyclone. There were no large pressure perturbations evident in the wall cloud (Fig. 9b). Only weak vertical motion was observed near wall cloud base (Fig. 9b). Stronger updraft at higher levels was observed within the wall cloud region, approaching magnitudes of 20 ms^{-1} at 2 km ARL (not shown).

5.2 Wall Cloud Parcel Source Regions

Parcel trajectories for the La Junta supercell wall cloud were calculated in the same manner as for the Goshen County supercell. The results are shown in Fig. 10. It is clear that most of the air entering wall cloud base is coming from the forward flank precipitation region of the storm (Fig. 10a, c). The trajectories suggest that the storms outflow was surging out ahead of the precipitation region. While some trajectories exhibited large vertical displacements at they moved toward the wall cloud (Fig.

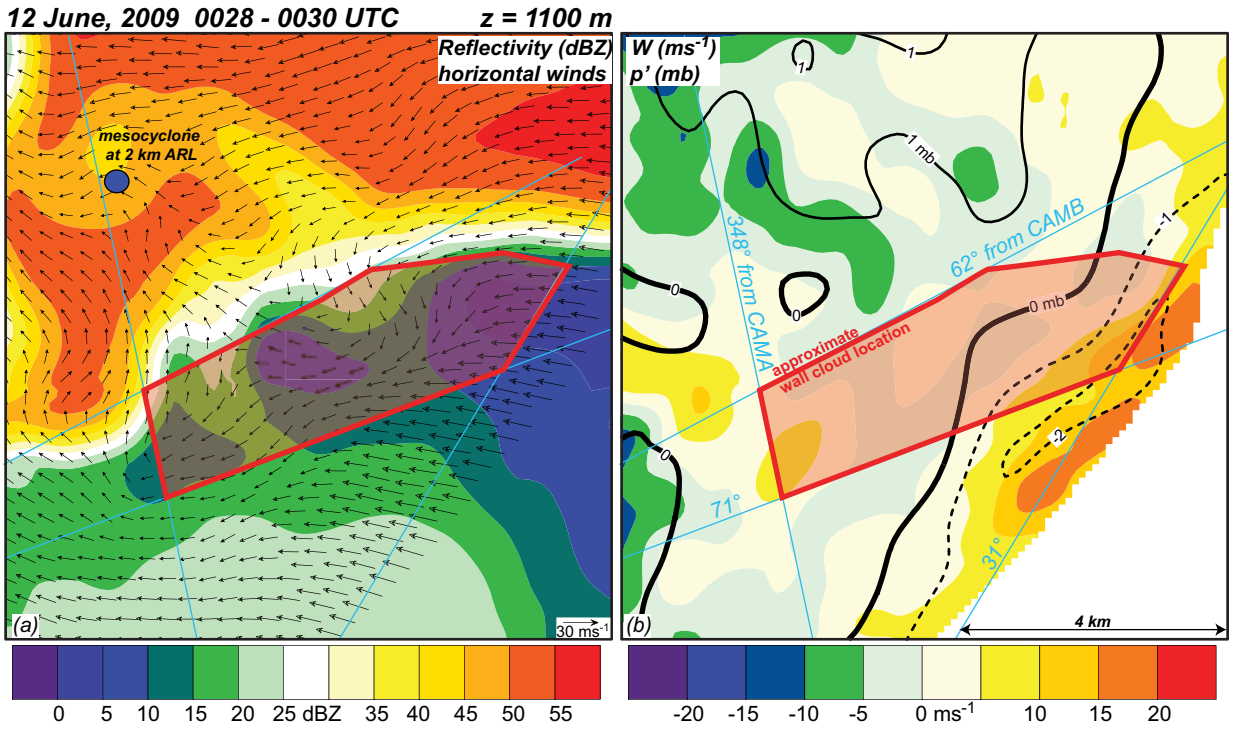

FIG 9. Dual-Doppler data from 0028:00 – 0030:00 UTC at 1100 m ARL is shown. (a) Radar reflectivity from DOW 7 (color) and dual-Doppler winds (ms^{-1}; black vectors). Cyan lines are the left and right azimuths of the estimated wall cloud location based on photogrammetry. The thick red line is the approximate wall cloud location. (b) Vertical velocity (ms^{-1}; color) and perturbation pressure (black contours) are shown. Wall cloud location and azimuths are same as in (a).

10b, d), the majority of the parcels ascended into wall cloud base and from the precipitation region. It is also clear from Fig. 10 that the there was only one source region of parcels entering the La Junta wall cloud. Unlike the Goshen County supercell, there appeared to be few or no parcels originating in the inflow or rear-flank downdraft regions of the La Junta supercell.

5.3 Wall Cloud Formation

Mobile mesonet data was again examined to approximate the thermodynamic properties of low-level parcels entering the wall cloud from the forward flank region. This data is summarized in Fig. 11. Notice that the air is cooler in the northeastern portion of the forward flank (light green observations) region and relatively warmer to the southwest (blue observations). The cooler parcels ascended into the northeastern portion of the wall cloud (Fig. 10a) where cloud base was lower (Fig. 8). The warmer parcels ascended into the higher, southwestern portion of the wall cloud. Computing mean potential temperature and mixing ratio values in the colder and warmer forward flank regions yielded cloud base heights of approximately 430 and 680 m, respectively. These cloud base heights are consistent with the phtogrammetrically-determined wall cloud base heights (Fig. 8). The observations shown in Figs. 8-11 suggest that the La Junta wall cloud formed as low-level parcels from the forward flank region ascended into the low-level updraft.

6. DISCUSSION AND SUMMARY

The formation of wall clouds observed within three supercells sampled by VORTEX2 has been examined. Results for two of the cases were presented herein. The first supercell occurred in Goshen County Wyoming on 5 June 2009 and produced an EF2 tornado. The Goshen County wall cloud was embedded in precipitation wrapping around the low-level mesocyclone. The wall cloud appeared to be centered on the low-level mesocyclone and

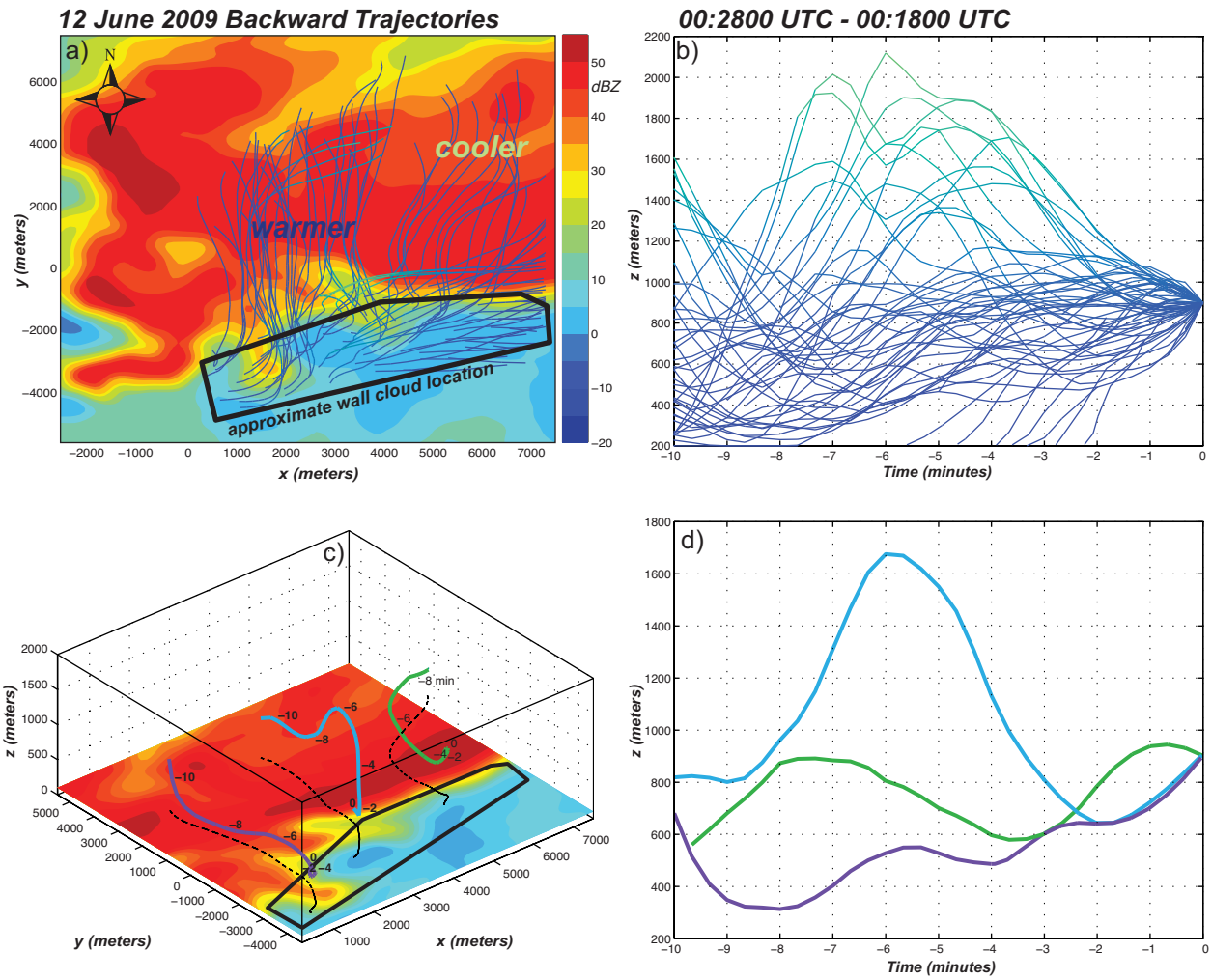

FIG 10. Radar reflectivity from DOW 7 (color; 1100 m ARL) and backward trajectories for parcels entering the wall cloud. The radar reflectivity data is from the 0028:00 – 0030:00 dual-Doppler analysis. Backward trajectories were calculated from 0028:00 to 0018:00 UTC. (a) Plan view of radar reflectivity and trajectories. The approximate wall cloud location is shown in black. (b) Height versus time plot of the trajectories shown in (a). (c) Three-dimensional perspective of the radar reflectivity field shown in (a) along with representative parcel trajectories. Black dashed lines represent the ground-relative location of the respective trajectories. Black time labels are minutes before the initial time of 0028:00 UTC. (d) Height versus time diagram of the three representative trajectories shown in (c).

therefore, contained strong rotation. A developing tornado was observed in the wall cloud. Air entering this wall cloud came from three source regions; the inflow, forward flank, and rear-flank downdraft. Most parcels originated in the forward flank region. The majority of the parcels from the inflow and forward flank regions originated at low levels. Some parcels in the forward flank originated at higher levels and descended into the wall cloud as did the rear-flank downdraft parcels. These wall cloud source regions were also observed with a wall cloud on 26 May 2010 that exhibited weak rotation (not shown).

The fact that some parcels reaching wall cloud base are descending in downdraft is perhaps not that surprising. Previous studies have shown that the low-level mesocyclone forms as horizontal vorticity is tilted at the updraft/downdraft interface. Furthermore, it has also been suggested that downdraft is necessary to abruptly tilt vortex lines vertically near the ground to produce a tornado. So, it is possible that tornadic wall clouds collocated with the low-level mesocyclone contain air that is descending in downdraft. It is not known how this air is descending. Perhaps high resolution modeling may

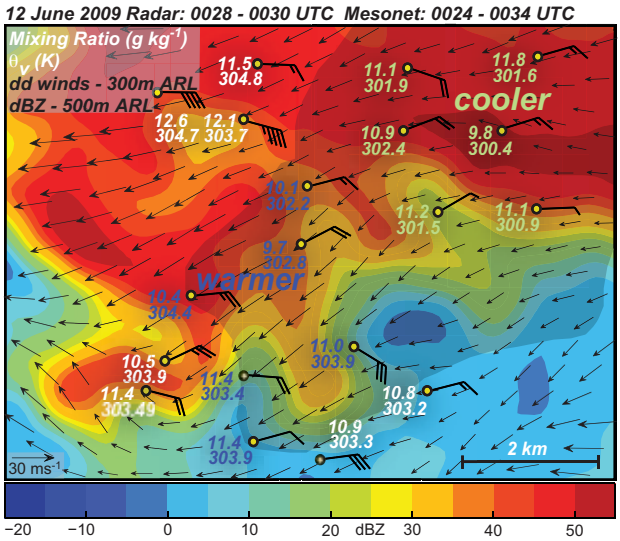

FIG 11. Radar reflectivity from DOW 7 (color; 500 m ARL) and dual-Doppler winds (black vectors; 300 m ARL) from 0028:00 – 0030:00 UTC on 12 June 2009. Mobile mesonet winds (black barbs; ½ flag = 5 ms^{-1}, full flag = 10 ms^{-1}), mixing ratio (g kg^{-1}), and virtual potential temperature (K) are shown from 0024:00 – 0034:00 UTC. The source region for parcels entering the wall cloud is shaded gray.

shed more light on the details of the forward and rear-flank downdrafts to address this question.

The observations suggested that the Goshen County wall cloud formed as low-level evaporatively-cooled air in the forward flank region ascended into the dynamically forced low-level updraft. Using mobile mesonet data to approximate the thermodynamic properties of the low-level forward flank parcels, saturation occurred at an altitude that was consistent with observed cloud base. This mechanism is consistent with that proposed by Rotunno and Klemp (1985). It was also shown that additional lowering may be attributed to the adiabatic cooling associated with the pressure deficit at the center of the rotating wall cloud.

A second wall cloud associated with a supercell west-northwest of La Junta CO on 11-12 June 2009 was examined. The La Junta wall cloud was well defined and extended approximately 700-800 m below the primary cloud base. The wall cloud formed on the southern periphery of the forward flank precipitation region. The outflow appeared to be surging away from the precipitation region. As a result, the wall cloud was not collocated with the mesocyclone.

Parcels entering wall cloud base appeared to come largely from the surging outflow. Many of the parcels originated at low-levels.

The La Junta wall cloud appeared to form from the lifting of evaporatively cooled forward flank parcels. Wall cloud base increased from northeast to southwest. This was a result of the forward flank downdraft being colder to the northeast. Parcel trajectories from this portion of the storm entered the northeastern portion of the wall cloud saturating at a lower altitude that the warmer parcels that ascended into the southwestern portion of the wall cloud.

There are important similarities and differences between the conclusions of Rotunno and Klemp (1985) and this study concerning wall clouds. Both studies have shown that wall clouds form as evaporatively-cooled air from the forward flank region ascends into the low-level dynamically forced updraft. This study has also shown that additional lowering may be attributed to the pressure deficit associated with strongly rotating wall clouds. Furthermore, it was shown herein that some parcels reaching wall cloud base may be descending from the forward flank region and rear-flank downdraft. Our analyses suggested that this will only be true for wall clouds that are collocated with the low-level mesocyclone.

Future work should examine more cases to assess the generality of these results. A modeling study would help to understand the important forcing mechanisms for parcels descending from the forward flank region and rear-flank downdraft. Finally, work is underway to examine the three-dimensional structure of wall clouds and their relationship with the storm updraft, precipitation region, and low-level mesocyclone.

Acknowledgments: This research was supported by the National Science Foundation under grants AGS-0757714 and AGS-1242339.

REFERENCES

Atkins, N. T., A. McGee, R. Ducharme, R. M. Wakimoto, and J. Wurman, 2012: The LaGrange tornado during VORTEX2. Part II: Photogrammetric analysis of the tornado combined with dual-Doppler radar data. *Mon. Wea. Rev.*, **140**, 2939 – 2958.

Bluestein, H. B., 1983: Surface meteorological observations in severe thunderstorms. Part II: Field experiments with TOTO. *J. Climate Appl. Meteor.*, **22**, 919–930.

——,1984: Photographs of the Canyon, Texas

storm on 26 May 1978. *Mon. Wea. Rev*., **112**, 2521–2523.

——, 1993: Synoptic-Dynamic Meteorology in Midlatitudes. Vol. 2, Observations and Theory of Weather Systems, Oxford Press, 594 pp.

Davies-Jones, R.P., 1986: Tornado dynamics. Vol. 2, Thunderstorms: A Social and Technological Documentary. 2d ed. E. Kessler, Ed., University of Oklahoma Press, 197–236.

Gal-Chen, T., 1978: A Method for the Initialization of the Anelastic Equations: Implications for Matching Models with Observations. *Mon. Wea. Rev*., **106**, 587–606.

Hane, C. E., P. S. Ray, 1985: Pressure and Buoyancy Fields Derived from Doppler Radar Data in a Tornadic Thunderstorm. *J. Atmos. Sci.*, **42**, 18–35.

Kosiba, K., J. Wurman, Y. Richardson, P. Markowski, P. Robinson, and J. Marquis, 2013: Genesis of the Goshen County, Wyoming, Tornado on 5 June 2009 during VORTEX2. *Mon. Wea. Rev.*, **141**, 1157–1181.

Lemon, L. R., and C. A. Doswell, 1979: Severe Thunderstorm Evolution and Mesocyclone Structure as Related to Tornadogenesis. *Mon. Wea. Rev*., **107**, 1184–1197.

Markowski, P., and Coauthors, 2012: The Pretornadic Phase of the Goshen County, Wyoming, Supercell of 5 June 2009 Intercepted by VORTEX2. Part I: Evolution of Kinematic and Surface Thermodynamic Fields. *Mon. Wea. Rev*., **140**, 2887–2915.

____, and Coauthors, 2012: The Pretornadic Phase of the Goshen County, Wyoming, Supercell of 5 June 2009 Intercepted by VORTEX2. Part II: Intensification of Low-Level Rotation. *Mon. Wea. Rev.*, **140**, 2916–2938.

____, M. Majcen, Y. Richardson, J. Marquis, and J. Wurman, 2011: Characteristics of the wind field in a trio of nontornadic low-level mesocyclones observed by the Doppler on Wheels radars. Electronic *J. Severe Storms Meteor*., **6** (3), 1–48.

Moller, A. R., 1978: The improved NWS storm spotters' training program at Ft. Worth, Tex. *Bull. Amer. Meteor. Soc*., **59**, 1574 – 1582.

Okubo, K., 1970: Horizontal dispersion of floatable particles in the vicinity of velocity singularities such as convergences. *Deep-Sea Res*., **17**, 445-454.

Rotunno, R., and J. B. Klemp, 1985: On the rotation and propagation of simulated supercell thunderstorms. *J. Atmos. Sci.,* **42**, 271–292.

Wakimoto, R.M., N. T. Atkins, and J. Wurman, 2011: The LaGrange tornado during VORTEX2. Part I: photogrammetric analysis of the tornado combined with single-Doppler radar data. *Mon. Wea. Rev.*, **139**, 2233–2258.

Waugh, S., and S. E. Fredrickson, 2010: An improved aspirated temperature system for mobile meteorological observations, especially in severe weather. Preprints, *25th Conf. on Severe Local Storms*, Denver, CO, Amer. Meteor. Soc., P5.2. [Available online at https://ams.confex.com/ams/25SLS/webprogram/Paper176205.html.]

Weiss, J., 1991: The dynamics of enstrophy transfer in two-dimensional hydrodynamics. *Physica D*, **48**, 273–294.

Wurman, J., 2001: The DOW mobile multiple-Doppler network. Preprints, *30th Int. Conf. on Radar Meteorology,* Munich, Germany, Amer. Meteor. Soc., P3.3.

____, D. Dowell, Y. Richardson, P. Markowski, E. Rasmussen, D. Burgess, L. Wicker, H. B. Bluestein, 2012: The Second Verification of the Origins of Rotation in Tornadoes Experiment: VORTEX2. *Bull. Amer. Meteor. Soc*., **93**, 1147–1170.